

The long-term spatio-temporal variability of sea surface temperature in the Northwest Pacific and the Near China Sea

Zhiyuan Wu ^{1,2,3}, Changbo Jiang ^{1,2}, Mack Conde ⁴, Jie Chen ^{1,2,*}, Bin Deng ^{1,2}

¹ School of Hydraulic Engineering, Changsha University of Science & Technology, Changsha, 410114, China;

² Key Laboratory of Water-Sediment Sciences and Water Disaster Prevention of Hunan Province, Changsha, 410114, China;

³ School for Marine Science and Technology, University of Massachusetts Dartmouth, New Bedford, MA 02744, USA;

⁴ School of Marine Science and Ocean Engineering, University of New Hampshire, Durham, NH 03824, USA.

* Correspondence: chenjie166@163.com

Abstract: The variability of the sea surface temperature (SST) in the Northwest Pacific has been studied on seasonal, annual and interannual scales based on the monthly datasets of ERSST 3b (1854-2017, 164 years) and OISST V2 (1988-2017, 30 years). The overall trends, spatial-temporal distribution characteristics, regional differences in seasonal trends, and seasonal differences of SST in the Northwest Pacific have been calculated over the past 164 years based on these datasets. In the past 164 years, the SST in the Northwest Pacific has been increasing linearly year by year with a trend of 0.033 °C/10 yr. The SST during the period from 1870 to 1910 is slow decreasing and staying in the range between 25.2 °C to 26.0 °C. During the period of 1910-1930, the SST as whole maintained a low value, which is at the minimum over the 164 years. After 1930, SST has continued to increase until now. The increasing trend in the past 30 years has reached 0.132 °C/10 yr and the increasing trend in the past 10 years is 0.306 °C/10 yr, which is around ten times in the past 164 years. The SST in most regions of the Northwest Pacific showed a linear increasing trend year by year, and the increasing trend in the offshore region was stronger than that in the ocean and deep-sea region. The change in trend of the SST in the Northwest Pacific shows a large seasonal difference, and the increasing trend in autumn and winter is larger than that in spring and summer. There are some correlations between the SST and some climate indices and atmospheric parameters, the correlation between the SST and some atmospheric parameters have been discussed, such as NAO, PDO, SOI anomaly, TCW, Nino 3.4, SLP, Precipitation, T2 and wind speed. The lowest SST in the Near China Sea basically occurred in February and the highest in August. The SST fluctuation in the Bohai Sea and Yellow Sea (BYS) is the largest with a range from 5 °C to 22 °C, the SST in the East China Sea (ECS) is from 18 °C to 27 °C, the smallest fluctuations occurs in the South China Sea (SCS) maintained at range of 26 °C to 29 °C. There are large differences between the mean and standard deviation in different sea regions.

Keywords: sea surface temperature; spatio-temporal distribution; interannual and interdecadal time scales; the Northwest Pacific

37 **1. Introduction**

38 The ocean is one of the important components of the ocean-atmosphere coupling system (Chelton
39 and Xie, 2010; Wu et al., 2019a,b, 2020). Relative to the atmosphere, the ocean has characteristics such
40 as slow change and large heat capacity (England et al., 2014). Because of the gradual changes in the ocean,
41 climate change at the interannual, decadal, and longer timescales may be closely related to the ocean
42 (Trenberth and Hurrell, 1994; Ault et al., 2009). The Sea Surface Temperature (SST) is the basis for the
43 interaction between the ocean and the atmosphere (Wu et al., 2019c,d), and it characterizes the combined
44 results of ocean heat content (Buckley et al., 2014; Griffies et al., 2015), dynamic processes (Takakura et
45 al., 2018). It is a very important parameter for climate change and ocean dynamics process, reflects sea-
46 air heat and water vapor exchange. Observations and numerical simulations show that large-scale sea
47 surface temperature anomalies of over 20° in longitude and latitude can cause significant changes in
48 atmospheric circulation, such as the El Niño and La Niña phenomena (Chen et al., 2016; Zheng et al.,
49 2016). During El Niño, the trade winds in the tropical East Pacific will be weakened, and the SST increased
50 significantly, which was 3~5°C higher than normal years. As a result, major changes have been made in
51 the atmospheric circulation and ocean circulation, which has caused the worldwide atmospheric and
52 marine environment and the abnormality of climate (Li et al., 2017).

53 The Northwest Pacific is particularly affected by the El Niño in the East Pacific and determines the
54 oceanic climate change in China (Hu et al., 2018). On one hand, climate change causes an increasing SST
55 in the northwestern Pacific, which increases the vertical stratification of the water, affects the atmospheric
56 circulation, and changes the intensity and period of coastal winds and upwelling. On the other hand, the
57 10-year periods Pacific Decadal Oscillation (PDO) and the El Niño-Southern Oscillation (ENSO) occur
58 on average every 2 to 7 years, resulting in large variations in upwelling (Xiao et al., 2015; Yang et al.,
59 2017; Xue et al., 2018). These factors will all lead to the impact on the marine environment in Chinese
60 coastal areas, causing land-based droughts, floods and climate disasters (Xu et al., 2018). Therefore, it is
61 very urgent to study the impact of climate change on SST in the Northwest Pacific and the Near China
62 Sea. As one of the main parameters of global climate change and one of the important characterizations
63 and predictors of El Niño, the study of SST changes is particularly important.

64 Previous scholars have done a lot of work on the changing trend of SST. According to the Fifth
65 Assessment Report (AR5) of the Intergovernmental Panel on Climate Change (IPCC), the global SST
66 warming trend was 0.064 °C/10 yr between 1880 and 2012 (Pachauri et al, 2014). In fact, many studies
67 have shown that the Pacific SST anomalous changes are closely related to global and regional climate
68 changes, and it has multi-scale temporal variations (Graham, 1994; Latif, 2006; Shakun and Shaman, 2009;
69 Li et al, 2014). In addition, the El Niño-Southern Oscillation (ENSO) and the Pacific Decadal Oscillation
70 (PDO), which are closely linked to global and regional climate change, are found in this area. Therefore,
71 the Pacific is one of the key ocean areas that scholars have studied for a long time (Bao and Ren, 2014;
72 Mei et al., 2015; Stuecker et al, 2015; Wills et al, 2018).

73 So far, two types of main meteorological SST datasets have been obtained: one based on measured
74 mid-resolution (1° -5°) 100-year datasets and the other based on satellite high-resolution (1-10km) decade

75 datasets (Wang et al., 2011; Smith et al., 2014; Huang et al., 2015, 2016; Diamond et al., 2015). The former
76 has rebuilt a time series of months over 150 years and the latter has accumulated over 30 years of time
77 series on a daily average basis (Tian et al., 2019). The existing climatic datasets already have conditions
78 for allowing the creation of a natural mode of change in SST in terms of duration and resolution (Liu et
79 al., 2017; Wang et al., 2018). With the continuous improvement of ocean observation technology and the
80 accumulation of satellite remote sensing data, the conditions for the scholars use the satellite data for short-
81 term climate change research have been met. In recent years, the research and discussion on the interannual
82 change of SST based on satellite remote sensing SST has attracted wide attention (Tang et al., 2003; Yang
83 et al., 2013; Zhang et al., 2015; Skirving et al., 2018).

84 Satellite remote sensing can achieve large-area simultaneous measurements with high temporal and
85 spatial resolution. The remote sensing SST obtained is conducive to a more comprehensive and rapid
86 understanding of oceanographic phenomena that affect the ocean surface, including El Niño (Robinson,
87 2016). At present, about 30 years of satellite remote sensing SST data have been accumulated (Franch et
88 al., 2017), and a set of sea surface temperature data has been provided to study the conditions for the
89 occurrence and development of ocean surface heat change modes in the temporal and spatial span and
90 resolution. So, satellite remote sensing SST has received widespread attention in recent years.

91 At present, based on satellite remote sensing data, the time scales for the study of changes in SST in
92 the Northwest Pacific, especially in the Near China Sea, are mostly within 20 years, which is relatively
93 short for studying climate change (Song et al., 2018; Pan et al., 2018). Most of the research is targeted at
94 specific local sea areas, and there is less research on the changes of the SST in the Northwest Pacific
95 covering all marginal seas of China. Therefore, it is necessary to study the SST variation of large-scale
96 and long-term sequences based on satellite remote sensing data.

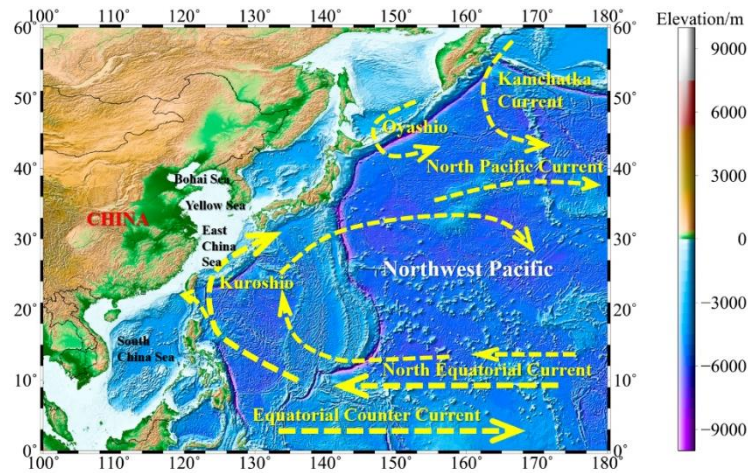
97 Previous scholars have made great contributions to the study of global warming, but most of them
98 are the overall changes in the regional average SST, and they tend to ignore the characteristics of changes
99 in certain key sea areas. There are great differences in the trends of SST in different sea areas. The long-
100 term trend of the SST changes in the Northwest Pacific (0° N- 60° N, 100° E- 180° E) over the past 164
101 years (1854-2017) have been calculated based on the monthly datasets of ERSST 3b in this study. The
102 temporal and spatial distribution characteristics of SST, the overall long-term trend, the regional variation
103 of the seasonal trend, and the seasonal differences were analyzed. The correlations with SST changes and
104 climate parameters and indices are been analyzed. To provide a reference for the study of global climate
105 change, the characteristics of SST changes in the Near China Sea has been studied in this paper.

106 High spatial resolution SST datasets including average SST field and monthly SSTA field are been
107 obtained. In view of the fact that there are many interannual and intra-annual changes, this paper analyzes
108 the characteristics of SST changes based on these datasets. The trend, inter-decadal changes in SST and
109 their causes, and the correlation with the climate parameters and indices such as Nino-3.4 index are
110 relatively low. The ocean thermal dynamic phenomenon is preliminarilly discussed. The datasets are
111 processed and analyzed to study the trend changes of the SST in the Northwest Pacific. To explore the
112 correlation and response mechanisms with climate systems such as the ENSO and the PDO, and to conduct
113 a detailed analysis of typical sea areas.

114 **2. Study region, Data and Methods**

115 *2.1. Study Region*

116 The Northwest Pacific is the northwest region of the Pacific, is defined as the offshore region of 0°N-
117 60°N and 100°E - 180°E in this study (Fig.1). There are more tropical cyclones over the Northwest Pacific
118 than any other sea area in the world, with an average annual average of 35. About 80% of these tropical
119 cyclones will develop into typhoons. On average, about 26 tropical cyclones per year reach at least the
120 intensity of tropical storms, accounting for about 31% of the global tropical storms, and more than double
121 the number of any other area. The sea-air interaction in this area is very strong and the change of SST is
122 worth to explore.



123
124 **Figure 1.** Bathymetric map of the Northwest Pacific and ocean circulation.

125 *2.2. SST Dataset*

126 Several data sources are used to analyze the long-term temporal and spatial variability of SST in the
127 Northwest Pacific in this present study. Long-term statistics are based on the monthly SST data from the
128 Extended Reconstructed Sea Surface Temperature (ERSST) 3b (1854-2017) (Smith et al., 2008). The
129 ERSST dataset is a global monthly sea surface temperature analysis derived from the International
130 Comprehensive Ocean–Atmosphere Dataset with missing data filled in by statistical methods. This
131 monthly analysis begins in January 1854 continuing to the present (<https://www1.ncdc.noaa.gov/pub/data/cmb/ersst/v3b/>). The primary SST dataset analyzed in this study is the NOAA Optimum
132 Interpolation (OI) Sea Surface Temperature (SST) V2 (OISST V2 1982-2017, <http://www.esrl.noaa.gov/psd/data/gridded/data.noaa.oisst.v2.html>) (Reynolds et al., 2002, 2007). There are many of SST data sets,
133 such as the HadISST1 data set replaces the GISST data sets, and is a unique combination of monthly
134 globally-complete fields of SST and sea ice Concentration on a 1 degree latitude-longitude grid from 1870
135 to date. But, from May 2007 the data set of in situ measurements used in HadISST has changed. The
136 advantage of this dataset is apparent when compared with other gridded datasets such as HadISST, ERSST
137 and OSTIA, which spans only the period since 2007.

138
139
140 The seasonal mean data are obtained by averaging the monthly average SST after the above-
141 mentioned processing. The spring is March, April and May (MAM), the summer is June, July and August

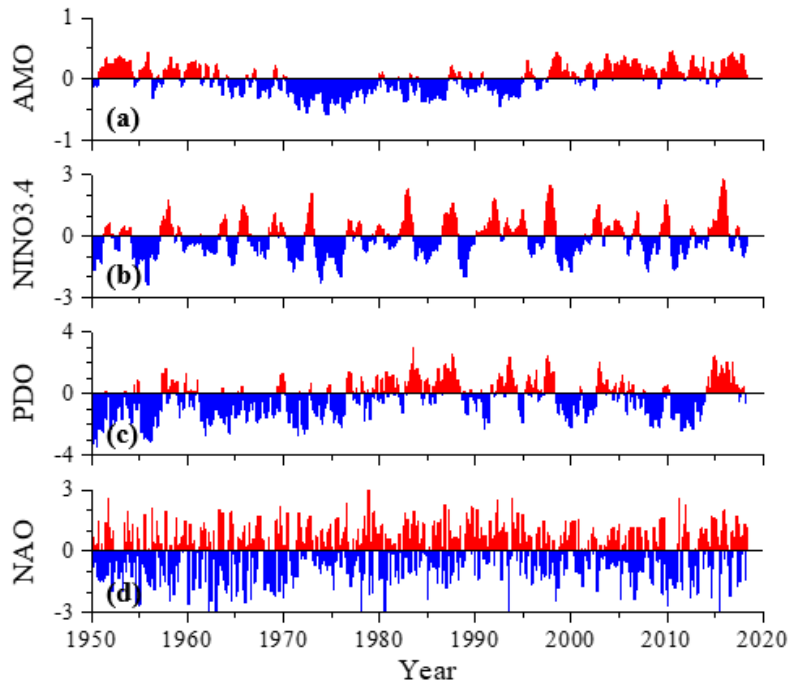
142 (JJA), the autumn is September, October and November (SON), and the winter is December of the
143 previous year and January and February (DJF).

144 The SST anomaly is the deviation from the long-term SST average of the observations of the SST
145 describing a particular area and time. The year anomaly represents the deviation of the average of the SST
146 for a given year from the mean of the multi-year SST. The month anomaly represents the deviation of the
147 average of the SST for a particular month from the average of the SST for that particular month for many
148 years. In this paper, the mean value from 1854 to 2017 is taken as the climate mean state, and the sea
149 surface temperature anomaly is subtracted from the SST field to obtain the SSTA field.

150 *2.3. Climate Index Dataset*

151 The Atlantic Multidecadal Oscillation (AMO) is a climate cycle that affects the sea surface
152 temperature (SST) of the North Atlantic Ocean based on different modes on multidecadal timescales
153 (<http://www.esrl.noaa.gov/psd/data/timeseries/AMO>, McCarthy et al, 2015). Niño 3.4 index uses SST to
154 characterize ENSO, the Niño 3.4 SST region consists of temperature measurements from between 5° N -
155 5° S and 120° - 170° W (Gergis and Fowler, 2005). The PDO index is the time coefficient of the first mode
156 obtained by performing EOF of the mean SSTA to the north of 20° N in the North Pacific
157 (<http://jisao.washington.edu/pdo/PDO.latest>). The North Atlantic Oscillation (NAO) is the most
158 prominent modality in the North Atlantic. Its climate impact is most prominent mainly in North America
159 and Europe, but it may also have an impact on the climate in other regions such as Asia. Recent studies
160 have not only further confirmed its existence, but also revealed its connection with a wide range of oceans
161 and atmospheric conditions.

162 The correlation between the SST and the atmospheric parameters is analyzed based on the ERA-
163 Interim data. ERA-Interim refers to the European Centre for Medium-Range Weather Forecasts (ECMWF),
164 which is an independent intergovernmental organization supported by 34 countries. Its goal is to develop
165 numerical methods for mid-term weather forecasting. The country provides forecasting services, conducts
166 scientific and technological research to accumulate forecasts, and accumulates meteorological data. ERA-
167 Interim is the latest global reanalysis product developed by ECMWF. The weather data and climate data
168 from January 1988 to December 2017 are used in this paper, such as sea surface temperature, sea-to-air
169 interface heat flux, and wind field data at a height of 10m, the spatial resolution of these datasets is
170 1.5°×1.5°.



171

172

Figure 2. AMO index (a), Niño 3.4 index (b), PDO index (c) and NAO index (d) during
173 1950~2017.

173

174 *2.4. Methods*

175

Regression analysis is an important part of mathematical statistics and multivariate statistics. It is a
176 mathematical method to study the correlation between variables and variables. The regression analysis has
177 a wide range of applications in the statistical forecasting of oceans and atmospheres. It is used to analyze
178 the statistical relationship between a variable (called forecast) and one or more independent variables
179 (called predict), and to establish a forecast. The regression equation produced by the quantity and forecast
180 factor, and then based on this equation to make predictions of the forecast volume. Regression analysis
181 includes linear regression and nonlinear regression. The linear regression is commonly used, and a linear
182 regression analysis method is used in this paper.

183

Use x_i to represent a climate variable with a sample size of n . Use t_i to represent the time
184 corresponding to x_i and establish a linear regression between x_i and t_i . The formula can be expressed as:

$$x_i = a + bt_i, \quad i = 1, 2, 3, \dots, n \quad (1)$$

185

Where, a is the regression constant and b is the regression coefficient. a and b can be calculated using
186 the least squares method.

187

For the observation data x_i and the corresponding time t_i , the least-squares calculation result of the
188 regression coefficient b and the constant a is expressed as:

$$b = \frac{\sum_{i=1}^n (x_i - \bar{x})(t_i - \bar{t})}{\sum_{i=1}^n (x_i - \bar{x})^2} \quad (2)$$

$$a = \bar{x} - b\bar{t}$$

189 The correlation coefficient between time t_i and x_i is:

$$r = \frac{\sqrt{\sum_{i=1}^n t_i^2 - \frac{1}{n} \left(\sum_{i=1}^n t_i \right)^2}}{\sqrt{\sum_{i=1}^n x_i^2 - \frac{1}{n} \left(\sum_{i=1}^n x_i \right)^2}} \quad (3)$$

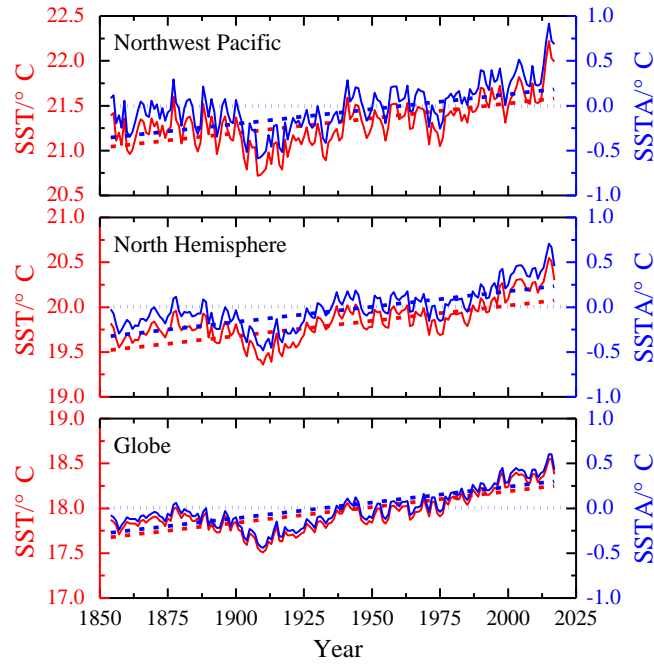
190 The correlation coefficient r is expressed as the degree of closeness of the linear correlation between
 191 the variable x and the time t . When $r > 0$, $b > 0$, indicating that x increases with time t ; when $r < 0$, $b < 0$,
 192 indicating that the variable x decreases with time t . A significance test is performed on the correlation
 193 coefficient to determine the significance level α (confidence is $1 - \alpha$) first. If $|r| > r_\alpha$, shows that the
 194 trend of the variable x with time t is significant, otherwise it is not significant.

195 3. Results and Discusses

196 3.1. Temporal distribution of SST

197 With the gradual warming of the global climate, the average temperature of the ocean is also rising.
 198 In order to reflect the overall trend of SST in the Northwest Pacific over the past 164 years (1854-2017),
 199 the average monthly SST data from 1854 to 2017 was used. The time series curve of SST in the Northwest
 200 Pacific, the Northern Hemisphere, and the global ocean was obtained by processing, and the overall trend
 201 of the SST was analyzed, as shown in Fig. 3. As can be seen from the figure, SST in the different region
 202 have shown an increasing trend and SST has shown a significant increasing trend since the 20th century.

203 The SST datasets were used to calculate the SST anomaly time series and its linear variation trend in
 204 the Northwest Pacific, the Northern Hemisphere and the global ocean as shown in Fig. 3. The slope of the
 205 linear equation with one unknown obtained by least-squares fitting is the annual change rate of SST, as
 206 shown in Table 1. It shows the increasing trend of SST at different time scales. It can be seen that the data
 207 shows that the SST in the different region has shown a significant warming trend as a whole. It can be
 208 seen from Table 1 that from 1854 to 2017, the SST trend of Northwest Pacific, North Hemisphere and
 209 global ocean has increased by 0.033 °C to 0.035 °C per 10 years. In the past 50 years, the increasing rate
 210 of SST has reached 0.10 °C/10 yr or more, and the increasing rate in the last 10 years has reached 0.30°C.
 211 It can be seen that the warming trend of SST in the Northwest Pacific is very significant.



212
213

Figure 3. The temporal variability of annual SST.

214

Table 1. The average trend of SST (Unit: °C/10 yr).

	NWP	NH	GLO
1854-2017 (164yr)	0.033	0.034	0.035
1918-2017 (100yr)	0.100	0.059	0.069
1968-2017 (50yr)	0.128	0.128	0.102
1988-2017 (30yr)	0.132	0.149	0.102
2008-2017 (10yr)	0.306	0.379	0.274

215 NWP: Northwest Pacific; NH: North Hemisphere; GLO: Globe. All the trend are significant at
216 the 95% confidence level.

217 There exist decadal to multi-decadal variations in the SST and SST anomalies series, with a general
218 cool period from the 1880s to 1910s, a weak warm period from 1920s to 1940s, a weak cool period from
219 1970s to 1980s, and a recent warm period from 1990s to present. Fig.3 also show that the interannual to
220 decadal variability is larger in the North Western Pacific, and it is smaller in the global ocean, indicating
221 an increase in SST anomaly variability with the area. It is also interesting to note that the latest 10 years
222 see a larger increasing trend of annual mean SST than that for the last 164 years, 100 years, 50 years and
223 30 years, indicating an obvious speed-up of warming of the Northwest Pacific, North Hemisphere and
224 globe ocean occurs in the last 10 years, and the growth rate over the past decade has been around ten times
225 that of the past 164 years.

226 In the past 164 years, the correlation coefficient of SST trends in the Northwest Pacific was 0.73. It
227 passed the 95% significance test, which shows that the linear trend is significant, and the regression
228 coefficient is 0.0033. This shows that in the past 164 years, the SST in the Northwest Pacific has been
229 increasing linearly year by year at a rate of 0.033 °C/10 yr. It can be seen from Fig. 3 that during the period

230 of 1870-1910, the SST slowly decreased, staying in the range between 25.2 °C to 26.0 °C; during the
231 period of 1910-1930, the SST as whole maintained a low value, and the change range was small, which is
232 at the minimum over the 164 years; since 1930, the SST has started to rise and the trend has continued to
233 this day.

234 In order to demonstrate the seasonal variation of the SST trend in the Northwest Pacific, the SST at
235 1°×1° at each grid point in the Northwest Pacific was averaged from 1854 to 2017 by winter, spring,
236 summer, autumn and year in this study. The season-by-season linear trend of SST at each grid point has
237 been analyzed. At the same time, the season-by-season time series of the SST anomalies were being
238 calculated and the seasonal variation of the comparison trends was shown in Fig 4.

239 Fig.4 (a) and (b) show seasonal and annual mean SST and SST anomalies series. The blue lines are
240 their trends of every seasonal mean SST and SST anomalies series for the Western Pacific during 1854-
241 2017, the red lines are their trends during 1988-2017. The increasing trends during 1854-2017 is between
242 0.032 °C/10 yr and 0.035 °C/10 yr for all seasons. The seasonal pattern for the latest 30 years shows a
243 more significant warming trend than that over the 164 year period. Significant warming occurs in all
244 seasons with those of autumn and winter being the largest, reaching 0.146 °C/10 yr and 0.124 °C/10 yr
245 respectively at the last 30 years, and that of spring the smallest.

246 An El Niño or La Niña event is identified if the NINO3.4 index exceeds +0.4°C for El Niño or -0.4°C
247 for La Niña, so ±0.4 °C is used for discriminating anomalies in this study. The magenta points mean the
248 SST anomaly larger than 0.4 °C, and the cyan points mean the SST anomaly is smaller than -0.4 °C in the
249 Fig.4 (b). As can be seen from the figure, during the period from 1890 to 1960, there were more negative
250 anomalies and less than -0.4 °C, indicating that there was a cool period during this period. In the period
251 from 1988 to 2017, there are more positive anomalies and more than 0.4 °C, indicating that there is a warm
252 period in the past 30 years.

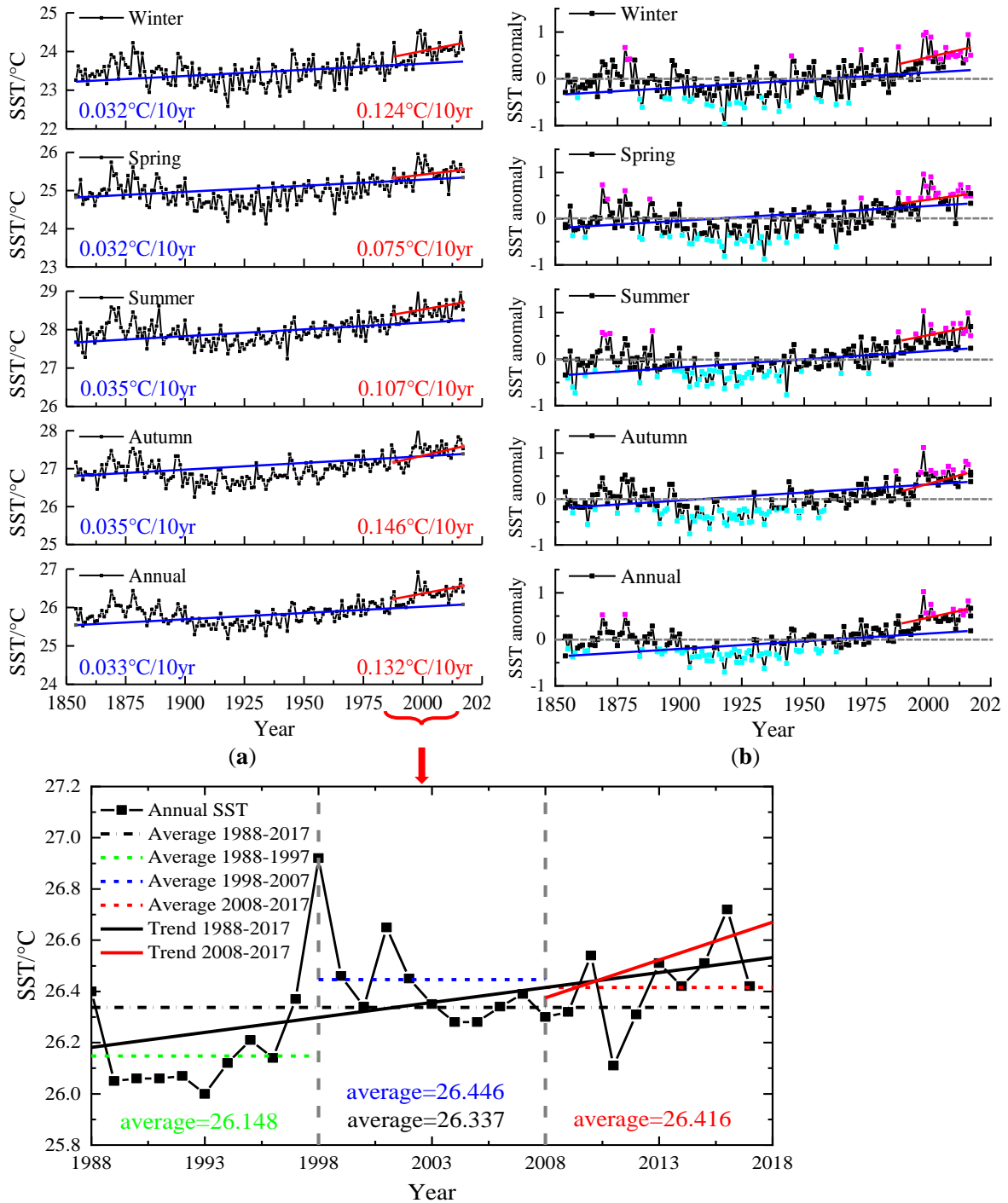
253 In the analysis of the SST changes in the Northwest Pacific during the past 164 years, it has been
254 found that there was a strong warming trend in SST over the past 30 years since 1988. It had been shown
255 that the SST in the Northwest Pacific has an overall warming trend since the 1970s in the previous studies
256 (Zhou et al., 2009; Kosaka et al., 2013) and this study. The time series of the SST in the Northwest Pacific
257 from 1988 to 2017 was plotted as shown in Fig. 4(c).

258 Yamamoto's (1986) method has been used to determine the extremum point, and the formula is:

$$R_{SN} = \frac{|\overline{X_1} - \overline{X_2}|}{S_1 + S_2} \quad (4)$$

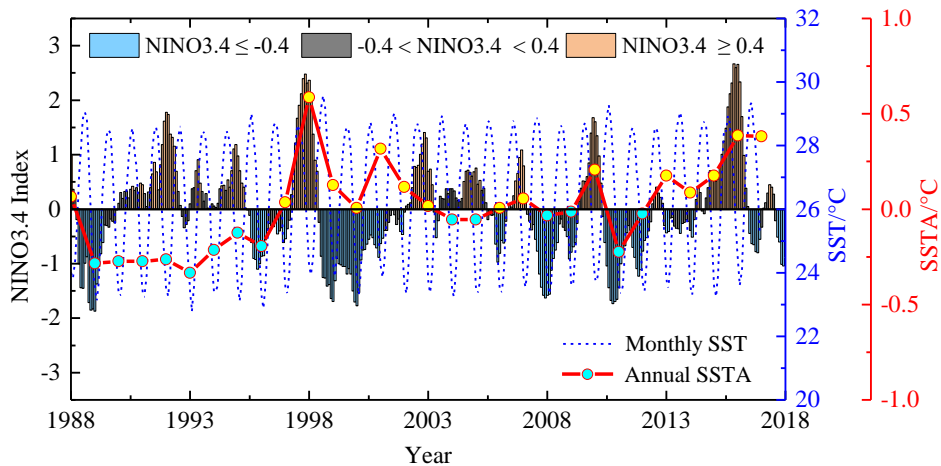
259 Where, $\overline{X_1}$, $\overline{X_2}$, S_1 , S_2 are the average and standard deviation of the two stages before and after
260 the extreme year. It was found that there were six stations when $X_1 = X_2 = 10$, $R_{SN} \geq 0.7$ in 10 years before
261 and after 1998/1999, and the significance level of the statistic reached $\alpha = 0.05$, according to which the
262 SST was considered to have a extremum in this year. The difference between the mean value of the
263 anomaly before and after the extreme was 0.30°C, and the similar results can also be seen in Fig. 4(c). It
264 can be found that in the past 30 years, the SST in the Northwest Pacific has significantly warmed up as a

265 whole. The highest annual mean SST appears in 1998, and the temperature undergoes a weak decreasing
 266 trend since then, but the average SST during 1998-2007 reaches 26.446 °C, which is higher than around
 267 0.3 °C during 1988-1997. In the last 30 years of SST in the Northwest Pacific, the increasing trend in the
 268 last 10 years is obviously greater than the trend in the last 30 years.



269
 270 **Figure 4.** Variability of seasonal/annual SST. (a) the annual SST over the 1854-2017 period; (b)
 271 the SST anomaly over the 1854-2017 period; (c) the SST over the 1988-2017 period (the latest
 272 30 years).

273 The monthly average sea surface temperature in the Northwest Pacific is represented by an undulating
 274 curve, as shown in the blue dashed line in Fig. 5, and the sea surface temperature anomaly is a red dotted
 275 line. The positive value is filled in yellow, and the negative value is filled in cyan. The NINO3.4 index is
 276 one of several El Niño/Southern Oscillation (ENSO) indicators based on sea surface temperatures.
 277 NINO3.4 is the average sea surface temperature anomaly in the region bounded by 5°N to 5°S, from
 278 170°W to 120°W. This region has large variability on El Niño time scales, and is close to the region where
 279 changes in local sea surface temperature are important for shifting the large region of rainfall typically
 280 located in the far western Pacific. An El Niño or La Niña event is identified if the 5-month running-average
 281 of the NINO3.4 index exceeds +0.4°C for El Niño or -0.4°C for La Niña for at least 6 consecutive months.



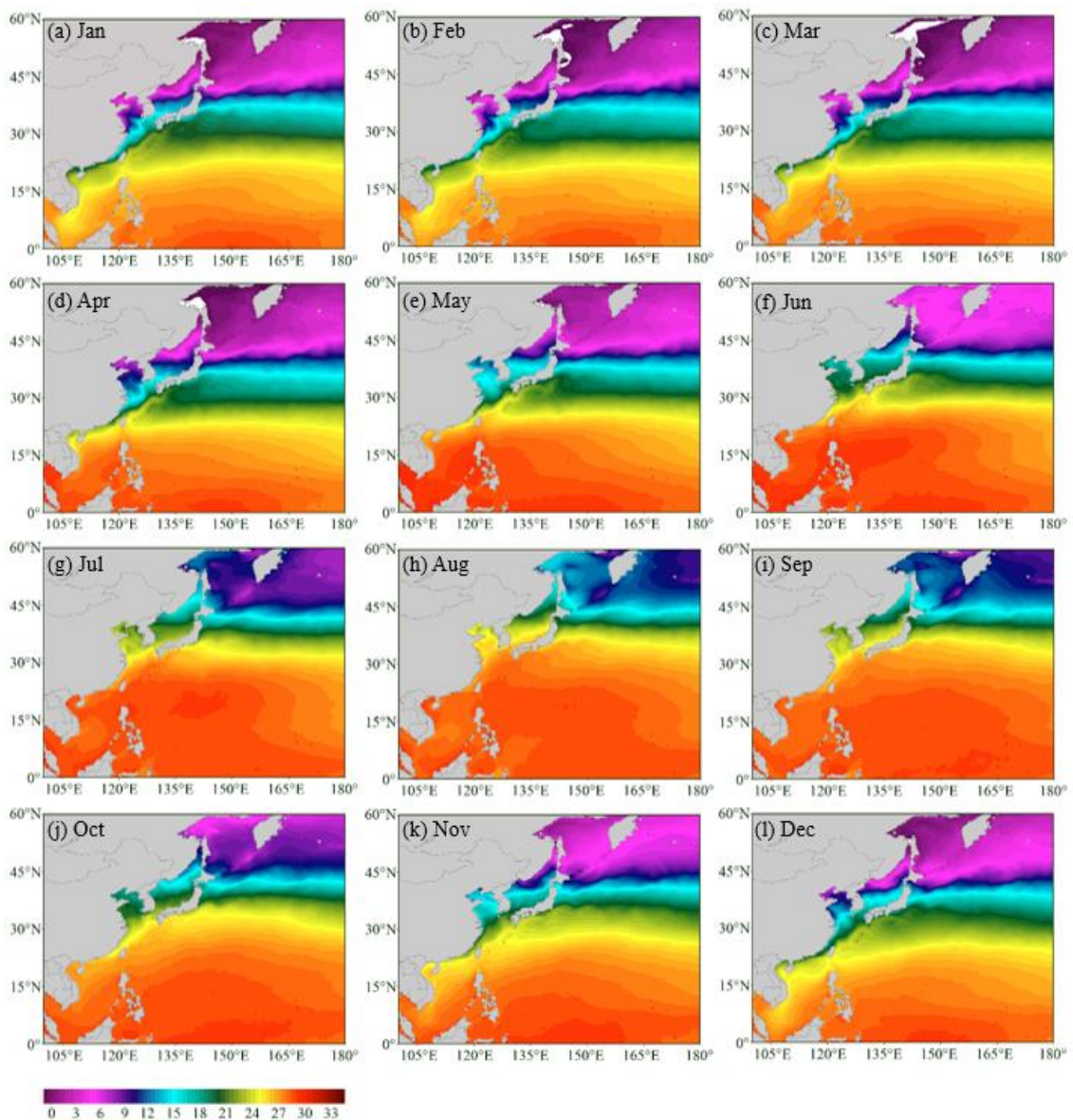
282
 283 **Figure 5.** The Nino 3.4 index and SST/SSTA during 1988 to 2017. (El Niño in pink and La
 284 Niña in blue.).

285 It can be seen from Fig.5 that the SSTA minimum value point occurs in 1989 to 1996; the maximum
 286 value point occurs in 1998 and 2016, and the maximum year coincides with the El Niño year. It is shown
 287 that the anomalous changes of the SST in the Northwest Pacific are closely related to the occurrence year
 288 of ENSO. The changes of the SST in the Northwest Pacific are obviously affected by the anomalous
 289 changes of SST in the Equatorial Pacific. The average SSTA was basically negative before 1996, and the
 290 basic value after it was positive. That is, the average SSTA was generally lower than the average of 1988-
 291 2017 before 1996, and the average SSTA after 1996 was basically higher than the average of 1988-2017,
 292 which is also reflected in Fig. 4(c).

293 In the low-latitude region, SST is more evenly distributed along the latitudes in January to April and
 294 November to December, and are higher in the south and lower in the north. From May to October, the
 295 distribution of SST along the latitude is tilted, showing the distribution characteristics of higher in the
 296 southwest and lower in the northeast, which is affected by the ocean circulation. In addition, as can also
 297 be seen in Fig. 6, in the low-latitude region, the SST range of change in different months is relatively small,
 298 between 27 °C to 33 °C, the change range of 5 °C to 6 °C. In the high-latitude region, the SST can be less
 299 than 3 °C at the lowest, and greater than 15°C at the highest, with a relatively large variation of more than
 300 12 °C.

301 3.2. Spatial distribution of SST

302 Fig. 6 shows the spatial distribution of the 30-year average SST for each month of 1988-2017. From
303 the figure, we can find that the spatial distribution of annual average SST in each month is similar, and the
304 SST is higher in the low-latitude (near equator) region and lower in the high-latitude region. In low-latitude
305 region, SST is more evenly distributed along the latitudes in January to April and November to December,
306 and are higher in the south and lower in the north. From May to October, the distribution of SST along the
307 latitude is tilted, showing the distribution characteristics of higher in the southwest and lower in the
308 northeast, which is affected by the ocean circulation. In addition, as can also be seen in Fig. 6, in the low-
309 latitude region, the SST range of change in different months is relatively small, between 27 °C to 33 °C,
310 the change range of 5 °C to 6 °C. In the high-latitude region, the SST can be less than 3 °C at the lowest,
311 and greater than 15°C at the highest, with a relatively large variation of more than 12 °C.

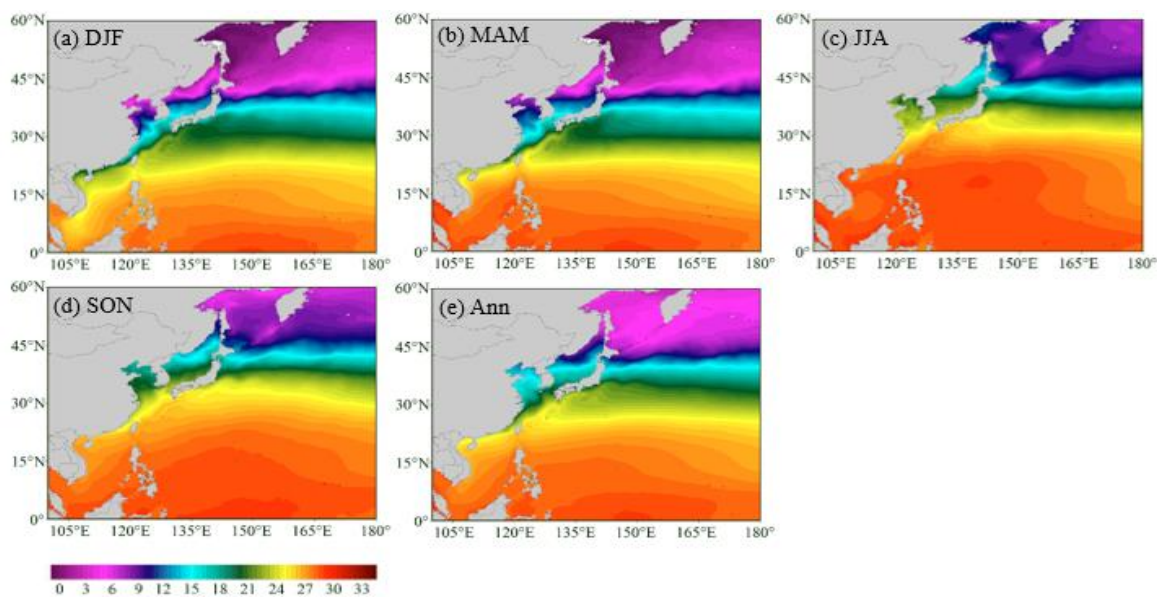


312

313

Figure 6. Spatial distribution of monthly SST over the 1988-2017 period.

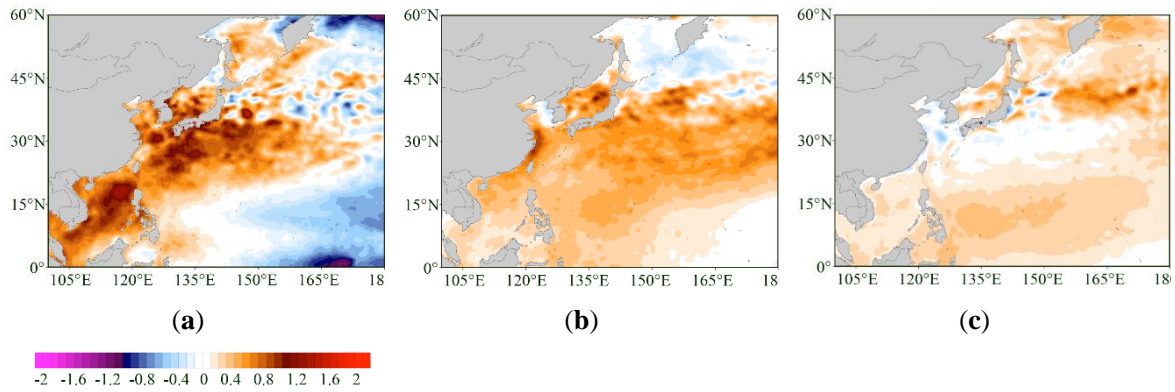
314 Fig.7 shows the spatial distribution of seasonal and annual mean SST during the 1988-2017 period.
 315 As can be seen from the figure, the spatial distribution of average SST in each season and annual is similar,
 316 and similar to the monthly results (Fig. 6). In the low-latitude region, the SST is higher, but in the high
 317 latitudes. SST is relatively low. Annual mean SST decreases with increasing latitude, with high
 318 temperature ranging from 26°C to 28°C in the south and low temperature ranging from 3°C to 6°C in the
 319 north, which is closely related to the solar radiation distribution in the deep-sea region. The isotherm is
 320 northeast–southwest oriented and the SST gradient increases as getting closer to the mainland coastal line.
 321 It is obvious that the landmass effect in the winter time has contributed to the tilting of the isotherms,
 322 which was pointed out by Bao et al (2014).



323
 324 **Figure 7.** Spatial distribution of seasonal/annual SST over the 1988-2017 period (a) Winter:
 325 DJF; (b) Spring: MAM; (c) Summer: JJA; (d) Autumn: SON (e) Annual.

326 Fig. 8 shows the results of SST anomaly in three characteristic stages. Fig. 8(a) shows the SST
 327 anomaly for the annual 1998 minus 1988-2017, Fig.8 (b) is the annual SST difference between the 10
 328 years after 1998 (1998-2007) and the previous 10 years (1988-1997) and Fig.8 (c) is the SST anomaly for
 329 the last 10 years (2008-2017) and the past 30 years (1988-2017).

330 It can be seen that there was a significant positive anomaly across the past 30-year average in 1998
 331 from Fig. 8(a). The positive anomalies around 1.0°C are shown in a large area in the Near China Sea,
 332 indicating that the SST is significantly warmer. In the southeast and northeast of the Northwest Pacific,
 333 negative anomalies have occurred in this region, and the lowest is close to -0.6°C, indicating that the SST
 334 has cooled in this region. The SSTA in the Northwest Pacific showed a trend of high in the west and low
 335 in the east. From the previous analysis, we found that this extremum is highly coincident with El Niño
 336 (Fig. 5). Therefore, it is likely that this phenomenon has been caused by the temperature difference and
 337 time difference caused by the transfer of high-temperature water in the Northeast Pacific to the Northwest
 338 Pacific under the combined influence of atmospheric circulation and ocean circulation.



339

340

341

Figure 8. (a) Ann 1998 minus 1988-2017; (b) Ann 1998-2007 minus 1988-1997; (c) Ann 2008-2017 minus 1988-2017.

342

343

344

345

346

347

It can be seen from Fig. 8(b) that the SST during the 10 years from 1998 to 2007 has significantly increased compared with the previous 10 years from 1988 to 1997. The positive anomaly occurs to be 0.4°C to 0.8°C in the south region of 40°N . In the 10 years since 1998, the SST in the region has increased by 0.4°C to 0.8°C over the previous 10 years. In the region between 45°N and 60°N , the effect is small and is maintained between -0.2°C and 0°C , indicating that the SST in this region has not changed substantially or slightly.

348

349

350

351

352

353

354

Fig. 8(c) shows the anomalous results of SST over the last 10 years (2008-2017) and relatively nearly 30 years (1988-2017). As can be seen from the figure, in addition to the Bohai Sea, the Yellow Sea, and the southern region of Japan, there is a wide range of positive anomaly in other regions, and the past 10 years have increased on average in the past 30 years. From Fig. 4(a) and (b), we have known that the increasing trend of SST over the past 30 years is around three to four times that of the rising trend of SST over the past 164 years. Therefore, the increasing trend of SST in the past 10 years is more significant, which is consistent with the results in Fig. 4(c) and Table 1.

355

3.3. Correlation between the SST and the atmospheric parameters

356

357

358

359

360

361

362

363

364

365

Based on monthly data from ERA-Interim, there is some correlation between SST and atmospheric parameters have been shown in Fig.9, all marked patterns are at the level of significance equal to 0.05. It can be seen from Fig. 9(a) that there is a non-significant correlation between SST and North Atlantic Oscillation (NAO), but in the South China Sea and around the region. It shows a weak negative correlation between South China Sea SST and NAO. The Pacific Decadal Oscillation (PDO) is an important factor of climate change of the Northwest Pacific, and it has a strong correlation with ENSO. The PDO has a great influence on the Asian monsoon and climate change in the Northwest Pacific and is closely related to ENSO. There is a significant negative correlation between SST and PDO can be seen from Fig. 9(b). The Niño-3.4 index is usually used to indicate the intensity of the El Niño/La Niña event. So there is a significant negative correlation between SST and the atmospheric parameters Niño 3.4 in Fig. 9(d).

366

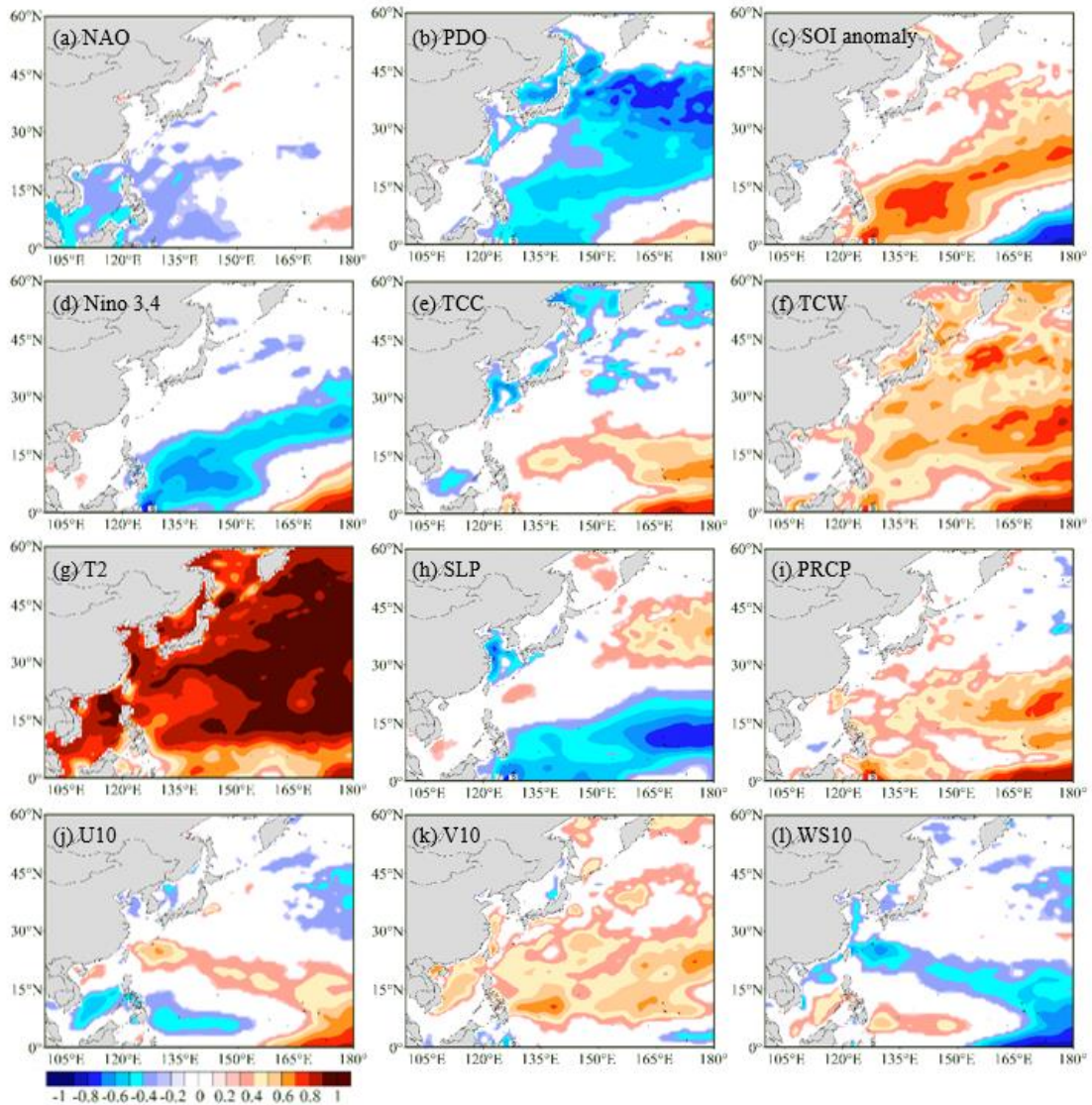
367

368

There is a significant positive correlation between SST and the Southern Oscillation Index (SOI) in Fig. 9(c), which is a standardized index based on the observed sea level pressure differences between Tahiti and Darwin, Australia. The monthly correlation between SST and T2 is high throughout the study

369 region, most markedly ($R>0.95$) over all Northwest Pacific. The effect of T2 on SST is significant over
 370 98% of the study region in all seasons. This is in good agreement with the previous studies (Skiriris et al,
 371 2012; Shaltout and Omstedt, 2014). Similarly, based on monthly data, there is a significant positive
 372 correlation between SST and Total Column Water (TCW), precipitation (PRCP).

373 The maximum negative correlation between the effect of Wind Speed 10m (WS10) on SST occurs
 374 southeast Northwest Pacific, and significant in an only small region. However, the direct correlation
 375 between V10 and SST is significant and positive over more of the Northwest Pacific.
 376



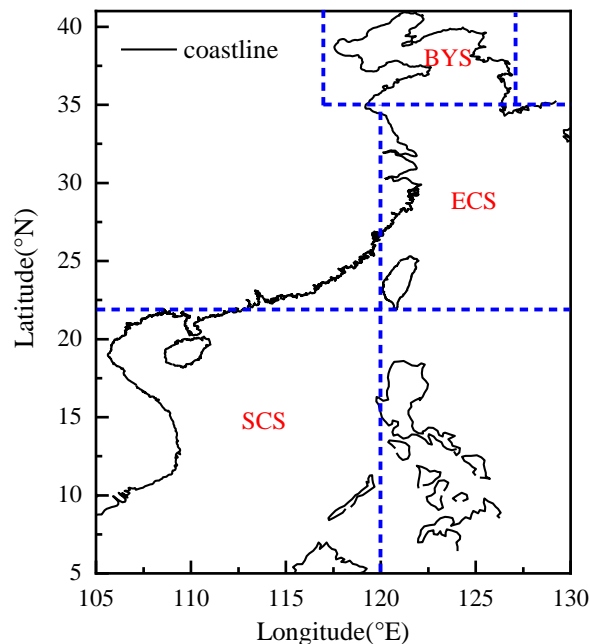
377
 378 **Figure 9.** The correlation coefficient between SST and the atmospheric components. (level of
 379 significance equal to 0.05).

380 *3.4. The Near China Sea SST characteristics*

381 The Near China Sea is defined as the four sea areas of the Bohai Sea, Yellow Sea, East China Sea,
 382 and South China Sea, and include the Kuroshio Extension, the part of Northwest Pacific and the sea

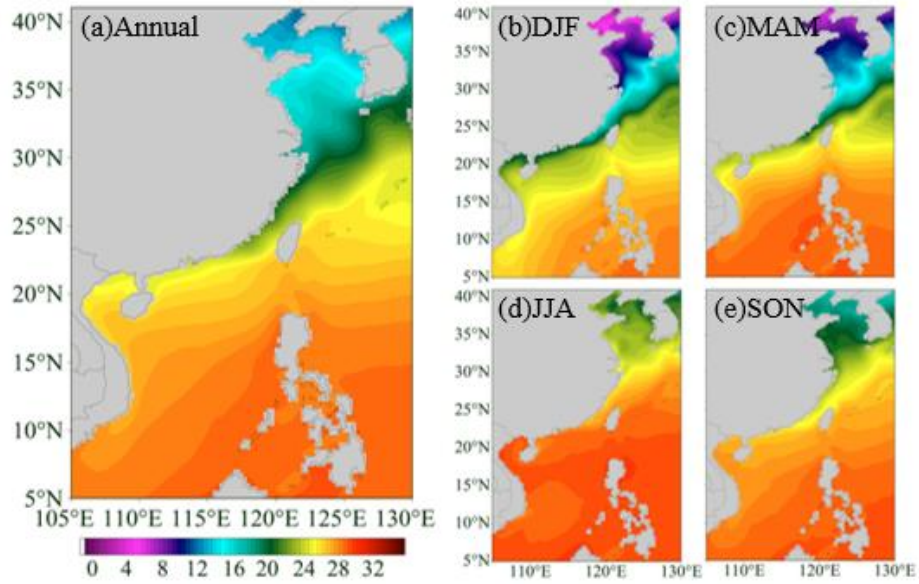
383 surrounding Japan in this study, which defined as the offshore region of 5°N-41°N and 105°E-130°E. The
384 changes in the average SST in the Yellow Sea and the Bohai Sea are very similar, so we analyze the two
385 sea areas together. Therefore, the region is further divided into three sub-regions: Bohai Sea and Yellow
386 Sea (BYS, 35°N-41°N and 117°E-127°E), East China Sea (ECS, 22°N-35°N and 120°E-130°E) and South
387 China Sea (SCS, 5°N-22°N and 105°E-120°E).

388 Fig.11 shows the spatial distribution of seasonal and annual mean SST in the Near China Sea during
389 the 1988-2017 period. Annual mean SST decreases with increasing latitude, with high temperature ranging
390 from 26°C to 28°C in the south and low temperature ranging from 14°C to 16°C in the north, which is
391 closely related to the solar radiation distribution in the offshore region. The isotherm is northeast–
392 southwest oriented and the SST gradient increases as getting closer to the mainland coastal line. It is
393 obvious that the landmass effect in the winter has contributed to the tilting of the isotherms, which was
394 pointed out by Bao et al. (2014). The ECS exhibits the largest temperature gradient, and the SCS in the
395 tropical zone the lowest temperature gradient.



396

397 **Figure 10.** Study regions defined in this paper. BYS: the Bohai Sea and the Yellow Sea; ECS:
398 the East China Sea; SCS: the South China Sea.

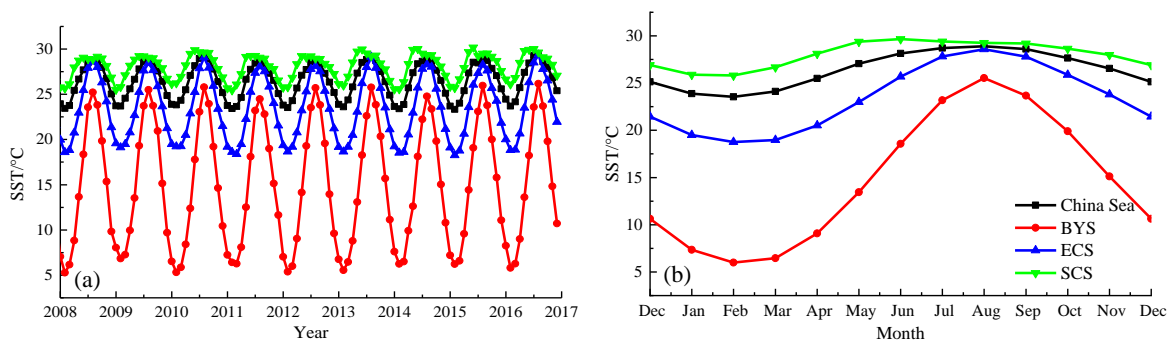


399
400
401

Figure 11. Annual (left) and seasonal (right) mean SST distribution during 1988-2017 in the China Sea. (a) Annual; (b) Winter: DJF; (c) Spring: MAM; (d) Summer: JJA; (e) Autumn: SON.

402
403
404
405
406
407
408
409

The monthly mean surface temperature changes over the past 10 years in the three regions (BYS, ECS and SCS) and the whole sea area (China Sea) are shown in Fig. 12. Fig. 12(a) shows the year-by-year variation of SST in different regions in the last 10 years, and Fig.12(b) shows the monthly SST variations in different regions in the past 10 years. The change variability of SST in different regions are basically synchronized. The minimum temperature basically occurs in February and the warmest occurs in August. The fluctuation range of SST in BYS is the largest, basically between 5 °C to 22 °C, from 18 °C to 27 °C in the East China Sea, and the smallest fluctuations is in the South China Sea, maintained at a range of 26 °C to 29 °C. There are large differences between the mean and standard deviation in different regions.



410
411
412
413

Figure 12. Long term monthly mean SST of the marginal seas of China during 2008-2017 (a) Yearly; (b) Monthly. Black line: China Sea; red line: Bohai Sea and Yellow Sea (BYS); blue line: East China Sea (ECS); green line: South China Sea (SCS).

414
415
416

Table 2 shows the annual and seasonal SST characteristics of the study area Near China Sea based on monthly data from 1988 to 2017. It can be found that in addition to the winter and spring in the BYS, the SST in each season of other regions shows an increasing trend from the table. Average increasing

417 trends of SST during 1988 to 2017 in BYS is 0.015 °C/ 10yr, 0.14 °C/ 10yr for the ECS, 0.12 °C/ 10yr for
 418 the SCS and 0.12 °C/ 10yr for whole Near China Sea respectively, and all the trends are significant at the
 419 99% confidence level. From the point of average annual SST, the SST in the South China Sea is the highest,
 420 reaching 28.01°C, followed by the East China Sea with 23.4°C, the lowest in the Bohai Sea and the Yellow
 421 Sea is 14.98°C, and the SST in the whole Near China Sea is 26.4°C. Table 3 shows the peak value and
 422 time of the annual and seasonal SST of the study area Near China Sea based on monthly data from 1988
 423 to 2017. In the past 30 years, colder SST occurs in 1989, 1990, 1992, 1993, 2003, 2008, 2010, 2011.
 424 Warmer SST occurs in 1997, 1998, 1999, 2001, 2015, 2016.
 425

426 **Table 2.** Annual and seasonal SST characteristics of the study area Near China Sea based on
 427 monthly data from 1988 to 2017.

	Average trend (°C/10yr)					Average (°C) ± standard deviation				
	Winter	Spring	Summer	Autumn	Annual	Winter	Spring	Summer	Autumn	Annual
BYS	-0.027	-0.097	0.084	0.13	0.015	8.08 ± 0.52	9.84 ± 0.49	22.44 ± 0.54	19.56 ± 0.44	14.98 ± 0.34
ECS	0.11	0.04	0.15	0.23	0.14	19.81 ± 0.33	20.87 ± 0.35	27.24 ± 0.31	25.66 ± 0.34	23.40 ± 0.26
SCS	0.13	0.10	0.11	0.14	0.12	26.09 ± 0.33	28.02 ± 0.27	29.38 ± 0.28	28.54 ± 0.27	28.01 ± 0.23
Whole	0.13	0.08	0.11	0.16	0.12	24.07 ± 0.27	25.53 ± 0.25	28.50 ± 0.24	27.50 ± 0.26	26.40 ± 0.21

428 **Table 3.** Peak value and time of the annual and seasonal SST of the study area Near China Sea
 429 based on monthly data from 1988 to 2017.

	Minimum (°C) and time (yr)					Maximum (°C) and time (yr)				
	Winter	Spring	Summer	Autumn	Annual	Winter	Spring	Summer	Autumn	Annual
BYS	7.13 (2003)	8.88 (2010)	21.13 (1993)	18.69 (1992)	14.45 (2010)	9.17 (2001)	11.02 (1998)	23.99 (1997)	20.70 (1998)	15.85 (1998)
ECS	19.30 (1989)	20.04 (2011)	26.76 (1993)	25.01 (1992)	22.97 (1993)	20.54 (1999)	21.84 (1998)	28.06 (2016)	26.43 (1998)	24.14 (1998)
SCS	25.53 (1993)	27.50 (2011)	28.97 (2008)	27.98 (1992)	27.68 (1989)	26.78 (2016)	28.53 (2001)	30.02 (1998)	29.14 (2015)	28.58 (1998)
Whole	23.61 (1993)	24.99 (2011)	28.18 (1990)	26.94 (1992)	26.07 (1993)	24.63 (1999)	26.05 (1998)	29.09 (1998)	28.18 (1998)	26.98 (1998)

430 4. Conclusions

431 The Northwest Pacific sea surface variability is affected by a combination of oceanic and atmospheric
 432 processes and displays significant regional and seasonal behavior. Monthly SST datasets based on ERSST
 433 3b (1854-2017, 164 years) and OISST V2 (1988-2017, 30 years) are used to make some long-term
 434 temporal and spatial variability statistics. The following conclusions can be drawn from the analysis.

435 In the last 164 years, SST in the Northwest has gradually increased, with an increasing trend of
436 0.033 °C/10 yr. Especially in the past 30 years, the increasing trend of SST reaches to 0.132 °C/10 yr, and
437 the increasing trend of SST reaches to 0.306 °C/10 yr in the last 10 years. The trend of the SST varies
438 seasonally. The increasing trend in winter and autumn are 0.124 °C/10 yr and 0.146 °C/10 yr respectively,
439 which are greater than spring and summer, with 0.075 °C/10 yr and 0.107°C /10 yr respectively. There
440 was an SST extremum point occurred around 1998, the average annual SST for the 10 years after 1998
441 increased by 0.3°C over the previous 10 years. It has been found that the change of SST/SSTA in the
442 Northwest Pacific is closely related to the ENSO through the statistical analysis of Nino3.4 index and
443 SST/SSTA.

444 From the perspective of spatial distribution, the annual mean SST decreases with increasing latitude,
445 with high temperature ranging from 27°C to 33°C in the south and low temperature ranging from 3°C to
446 15°C in the north. The SST is higher in the low-latitude (near equator) region and lower in the high-latitude
447 region. In the low-latitude region, SST is more evenly distributed along the latitudes in November to April,
448 but from May to October, the distribution of SST along the latitude is tilted, showing the distribution
449 characteristics of higher in the southwest and lower in the northeast, which is affected by the ocean
450 circulation.

451 There are many correlations between the SST and some climate indices and atmospheric parameters,
452 such as Pacific Decadal Oscillation (PDO), Southern Oscillation Index (SOI), Nino 3.4, total water vapor
453 column (TCW), temperature at 2 meters (T2), sea level pressure (SLP), precipitation (PRCP) and wind
454 speed at 10 meters (U10, V10 and WS10). A very significant positive correlation between SST and T2,
455 TCW was been found, of which the correlation coefficient between SST and T2 exceeded 98%. PDO,
456 Nino 3.4 is negatively correlated with SST, and the correlation between other indices and parameters and
457 SST is weak.

458 The whole Near China Sea was divided into three sections to analysis its spatial variability in a
459 different region, which is the Bohai Sea and Yellow Sea (BYS), East China Sea (ECS) and South China
460 Sea (SCS). The SST in the BYS is coolest with a range from 5 °C to 22 °C, and the warmest in the SCS
461 with a range from 26 °C to 29 °C. It can be seen from the statistical data that in addition to the winter and
462 spring in the BYS, SST in other regions and time had shown a warming trend. In the past 30 years, the
463 trend of SST increase of BYS was 0.015 °C/10 yr, while that of ECS and SCS was 0.14 °C/10 yr and
464 0.12 °C/10 yr, respectively.

465 **Competing interests:** The authors declare that they have no conflict of interest.

466 **Financial support:** The study was supported by the National Natural Science Foundation of China (Grant
467 Nos. 51809023, 51839002 and 51879015). The Partial Support also comes from the Research Foundation
468 of Education Bureau of Hunan Province, China (Grant Nos. 19C0092).

469 **Acknowledgements:** Most climate data were sourced from websites of the Climate Reanalyzer
470 (<https://climatereanalyzer.org>), produced by the Climate Change Institute at the University of Maine.

471 **References:**

- 472 Ault, T. R., Cole, J. E., Evans, M. N., Barnett, H., Abram, N. J., Tudhope, A. W., and Linsley, B. K.:
473 Intensified decadal variability in tropical climate during the late 19th century, *Geophysical Research*
474 *Letters*, 36, L08602, <https://doi.org/10.1029/2008GL036924>, 2009.
- 475 Bao, B., and Ren, G.: Climatological characteristics and long-term change of SST over the marginal seas
476 of China, *Continental Shelf Research*, 77, 96-106, <https://doi.org/10.1016/j.csr.2014.01.013>, 2014.
- 477 Buckley, M. W., Ponte, R. M., Forget, G., and Heimbach, P.: Low-frequency SST and upper-ocean heat
478 content variability in the North Atlantic, *Journal of Climate*, 27, 4996-5018,
479 <https://doi.org/10.1175/JCLI-D-13-00316.1>, 2014.
- 480 Chelton, D. B., and Xie, S. P.: Coupled ocean-atmosphere interaction at oceanic mesoscales,
481 *Oceanography*, 23, 52-69, <https://doi.org/10.5670/oceanog.2010.05>, 2010.
- 482 Chen, Z., Wen, Z., Wu, R., Lin, X., and Wang, J.: Relative importance of tropical SST anomalies in
483 maintaining the Western North Pacific anomalous anticyclone during El Niño to La Niña transition
484 years, *Climate dynamics*, 46, 1027-1041, <https://doi.org/10.1007/s00382-015-2630-1>, 2016.
- 485 Diamond, M. S., and Bennartz, R.: Occurrence and trends of eastern and central Pacific El Niño in different
486 reconstructed SST data sets, *Geophysical Research Letters*, 42, 10375–10381,
487 <https://doi.org/10.1002/2015GL066469>, 2015.
- 488 England, M. H., McGregor, S., Spence, P., Meehl, G. A., Timmermann A., Cai W., Gupta A. S., McPhaden
489 M. J., Purich A., and Santoso A.: Recent intensification of wind-driven circulation in the Pacific and
490 the ongoing warming hiatus, *Nature Climate Change*, 4, 222, <https://doi.org/10.1038/nclimate2106>,
491 2014.
- 492 Franch, B., Vermote, E.F., Roger, J.-C., Murphy, E., Becker-Reshef, I., Justice, C., Claverie, M., Nagol,
493 J., Csizsar, I., Meyer, D., Baret, F., Masuoka, E., Wolfe, R., and Devadiga, S.: A 30+ Year AVHRR
494 Land Surface Reflectance Climate Data Record and Its Application to Wheat Yield Monitoring,
495 *Remote Sensing*, 9, 296, <https://doi.org/10.3390/rs9030296>, 2017.
- 496 Gergis, J. L., and Fowler, A. M.: Classification of synchronous oceanic and atmospheric El Niño-Southern
497 Oscillation (ENSO) events for palaeoclimate reconstruction, *International Journal of Climatology*,
498 25, 1541-1565, <https://doi.org/10.1002/joc.1202>, 2005.
- 499 Graham, N. E.: Decadal-scale climate variability in the tropical and North Pacific during the 1970s and
500 1980s: Observations and model results, *Climate Dynamics*, 10, 135-162,
501 <https://doi.org/10.1007/BF00210626>, 1994.
- 502 Griffies, S. M., Winton, M., Anderson, W. G., Benson, R., Delworth, T. L., Dufour, C. O., Dunne, J. P.,
503 Goddard, P., Morrison, A. K., Rosati, A., Wittenberg, A. T., Yin, J., and Zhang R.: Impacts on ocean
504 heat from transient mesoscale eddies in a hierarchy of climate models, *Journal of Climate*, 28, 952-
505 977, <https://doi.org/10.1175/JCLI-D-14-00353.1>, 2015.
- 506 Hu, H., Wu, Q., and Wu, Z.: Influences of two types of El Niño event on the Northwest Pacific and tropical
507 Indian Ocean SST anomalies, *Journal of Oceanology and Limnology*, 36, 33-47,
508 <https://doi.org/10.1007/s00343-018-6296-5>, 2018.

509 Huang, B., Banzon, V. F., Freeman, E., Lawrimore, J., Liu, W., Peterson, T. C., Smith, T. M., Thorne, P.
510 W., Woodruff S. D., and Zhang, H. M.: Extended reconstructed sea surface temperature version 4
511 (ERSST. v4). Part I: upgrades and intercomparisons, *Journal of climate*, 28, 911-930,
512 <https://doi.org/10.1175/JCLI-D-14-00006.1>, 2015.

513 Huang, B., Thorne, P. W., Smith, T. M., Liu, W., Lawrimore, J., Banzon, V. F., and Menne, M. Further
514 exploring and quantifying uncertainties for extended reconstructed sea surface temperature (ERSST)
515 version 4 (v4), *Journal of Climate*, 29, 3119-3142, <https://doi.org/10.1175/JCLI-D-15-0430.1>, 2016.

516 Kosaka, Y., and Xie, S. P.: Recent global-warming hiatus tied to equatorial Pacific surface cooling, *Nature*,
517 501, 403, <https://doi.org/10.1038/nature12534>, 2013.

518 Latif, M.: On North Pacific multidecadal climate variability, *Journal of climate*, 19, 2906-2915,
519 <https://doi.org/10.1175/JCLI3719.1>, 2006.

520 Li, G., Li, C., Tan, Y., and Bai, T. The interdecadal changes of south pacific sea surface temperature in
521 the mid-1990s and their connections with ENSO, *Advances in Atmospheric Sciences*, 31, 66-84,
522 <https://doi.org/10.1007/s00376-013-2280-3>, 2014.

523 Li, X., Zong, Y., Zheng, Z., Huang, G., and Xiong, H.: Marine deposition and sea surface temperature
524 changes during the last and present interglacials in the west coast of Taiwan Strait, *Quaternary*
525 *International*, 440, 91-101, <https://doi.org/10.1016/j.quaint.2016.05.023>, 2017.

526 Liu, C., Sun, Q., Xing, Q., Liang, Z., Deng, Y., and Zhu, L.: Spatio-temporal variability in sea surface
527 temperatures for the Yellow Sea based on MODIS dataset, *Ocean Science Journal*, 52, 1-10,
528 <https://doi.org/10.1007/s12601-017-0006-7>, 2017.

529 McCarthy, G. D., Haigh, I. D., Hirschi, J. J. M., Grist, J. P., and Smeed, D. A.: Ocean impact on decadal
530 Atlantic climate variability revealed by sea-level observations, *Nature*, 521, 508,
531 <https://doi.org/10.1038/nature14491>, 2015.

532 Mei, W., Xie, S. P., Primeau, F., McWilliams, J. C., and Pasquero, C.: Northwestern Pacific typhoon
533 intensity controlled by changes in ocean temperatures, *Science Advances*, 1, e1500014,
534 <https://doi.org/10.1126/sciadv.1500014>, 2015.

535 Pachauri, R. K., Allen, M. R., Barros, V. R., Broome, J., Cramer, W., Christ, R., Church, J. A., Clarke, L.,
536 Dahe, Q., Dasgupta, P., Dubash, N. K., et al.: *Climate Change 2014: Synthesis Report. Contribution*
537 *of Working Groups I, II and III to the Fifth Assessment Report of the Intergovernmental Panel on*
538 *Climate Change / R. Pachauri and L. Meyer (editors)*, Geneva, Switzerland, IPCC, ISBN: 978-92-
539 9169-143-2, 2014.

540 Pan, X., Wong, G. T., Ho, T. Y., Tai, J. H., Liu, H., Liu, J., and Shiah, F. K.: Remote sensing of surface
541 [nitrite+ nitrate] in river-influenced shelf-seas: The northern South China Sea Shelf-sea, *Remote*
542 *Sensing of Environment*, 210, 1-11, <https://doi.org/10.1016/j.rse.2018.03.012>, 2018.

543 Reynolds, R. W., Rayner, N. A., Smith, T. M., Stokes, D. C., and Wang, W.: An improved in situ and
544 satellite SST analysis for climate, *Journal of climate*, 15: 1609-1625, [https://doi.org/10.1175/1520-](https://doi.org/10.1175/1520-0442(2002)015)
545 [0442\(2002\)015](https://doi.org/10.1175/1520-0442(2002)015), 2002.

546 Reynolds, R. W., Smith, T. M., Liu, C., Chelton, D. B., Casey, K. S., and Schlax, M. G.: Daily high-
547 resolution-blended analyses for sea surface temperature, *Journal of Climate*, 20, 5473-5496,
548 <https://doi.org/10.1175/2007JCLI1824.1>, 2007.

549 Robinson, C. J.: Evolution of the 2014–2015 sea surface temperature warming in the central west coast of
550 Baja California, Mexico, recorded by remote sensing, *Geophysical Research Letters*, 43, 7066-7071,
551 <https://doi.org/10.1002/2016GL069356>, 2016.

552 Shakun, J. D., and Shaman, J.: Tropical origins of North and South Pacific decadal variability, *Geophysical*
553 *Research Letters*, 36, L19711, <https://doi.org/10.1029/2009GL040313>, 2009,

554 Shaltout, M., and Omstedt, A.: Recent sea surface temperature trends and future scenarios for the
555 Mediterranean Sea, *Oceanologia*, 56, 411-443, <https://doi.org/10.5697/oc.56-3.411>, 2014.

556 Skirving, W., Enríquez, S., Hedley, J.D., Dove, S., Eakin, C.M., Mason, R.A.B., De La Cour, J.L., Liu,
557 G., Hoegh-Guldberg, O., Strong, A.E., Mumby, P.J., and Iglesias-Prieto, R.: Remote Sensing of Coral
558 Bleaching Using Temperature and Light: Progress towards an Operational Algorithm, *Remote*
559 *Sensing*, 10, 18, <https://doi.org/10.3390/rs10010018>, 2018.

560 Skliris, N., Sofianos, S., Gkanasos, A., Mantziafou, A., Vervatis, V., Axaopoulos, P., and Lascaratos, A.:
561 Decadal scale variability of sea surface temperature in the Mediterranean Sea in relation to
562 atmospheric variability, *Ocean Dynamics*, 62, 13-30, <https://doi.org/10.1007/s10236-011-0493-5>,
563 2012.

564 Smith, C. A., Compo, G. P., and Hooper, D. K.: Web-Based Reanalysis Intercomparison Tools (WRIT)
565 for analysis and comparison of reanalyses and other datasets, *Bulletin of the American*
566 *Meteorological Society*, 95, 1671-1678, <https://doi.org/10.1175/BAMS-D-13-00192.1>, 2014.

567 Smith, T. M., Reynolds, R. W., Peterson, T. C., and Lawrimore, J.: Improvements to NOAA’s historical
568 merged land–ocean surface temperature analysis (1880–2006), *Journal of Climate*, 21, 2283-2296,
569 <https://doi.org/10.1175/2007JCLI2100.1>, 2008.

570 Stuecker, M. F., Jin, F. F., Timmermann, A., and McGregor, S. Combination mode dynamics of the
571 anomalous northwest Pacific anticyclone, *Journal of Climate*, 28, 1093-1111,
572 <https://doi.org/10.1175/JCLI-D-14-00225.1>, 2015.

573 Song, D., Duan, Z., Zhai, F., and He, Q.: Surface diurnal warming in the East China Sea derived from
574 satellite remote sensing, *Chinese Journal of Oceanology and Limnology*, 36, 620–629,
575 <https://doi.org/10.1007/s00343-018-7035-7>, 2018.

576 Takakura, T., Kawamura, R., Kawano, T., Ichiyanagi, K., Tanoue, M., and Yoshimura, K.: An estimation
577 of water origins in the vicinity of a tropical cyclone’s center and associated dynamic processes,
578 *Climate Dynamics*, 50, 555-569, <https://doi.org/10.1007/s00382-017-3626-9>, 2018.

579 Tang, D., Kester, D. R., Wang, Z., Lian, J., and Kawamura, H. AVHRR satellite remote sensing and
580 shipboard measurements of the thermal plume from the Daya Bay, nuclear power station, China,
581 *Remote Sensing of Environment*, 84, 506-515, [https://doi.org/10.1016/S0034-4257\(02\)00149-9](https://doi.org/10.1016/S0034-4257(02)00149-9),
582 2003.

583 Tian, F., von Storch, J. S., and Hertwig, E.: Impact of SST diurnal cycle on ENSO asymmetry[J]. *Climate*
584 *Dynamics*, 52, 2399–2411, <https://doi.org/10.1007/s00382-018-4271-7>, 2019.

585 Trenberth, K. E., and Hurrell, J. W.: Decadal atmosphere-ocean variations in the Pacific, *Climate*
586 *Dynamics*, 9, 303-319, <https://doi.org/10.1007/BF00204745>, 1994.

587 Wang, C., Zou, L., and Zhou, T.: SST biases over the Northwest Pacific and possible causes in CMIP5
588 models, *Science China Earth Sciences*, 61, 1-12, <https://doi.org/10.1007/s11430-017-9171-8>, 2018.

589 Wang, Y., Liu, P., Li, T., and Fu, Y.: Climatologic comparison of HadISST1 and TMI sea surface
590 temperature datasets, *Science China Earth Sciences*, 54, 1238-1247, <https://doi.org/10.1007/s11430-011-4214-1>, 2011.

592 Wills, R. C., Schneider, T., Wallace, J. M., Battisti, D. S., and Hartmann, D. L.: Disentangling global
593 warming, multidecadal variability, and El Niño in Pacific temperatures, *Geophysical Research*
594 *Letters*, 45, 2487-2496, <https://doi.org/10.1002/2017GL076327>, 2018.

595 Wu, Z., Chen, J., Jiang, C., Liu, X., Deng, B., Qu, K., He, Z., and Xie, Z.: Numerical investigation of
596 Typhoon Kai-tak (1213) using a mesoscale coupled WRF-ROMS model — Part II: Wave effects,
597 *Ocean Engineering*, <https://doi.org/10.1016/j.oceaneng.2019.106805>, 2020.

598 Wu, Z., Jiang, C., Deng, B., Chen, J., Long, Y., Qu, K., and Liu, X.: Simulation of Typhoon Kai-tak using
599 a mesoscale coupled WRF-ROMS model, *Ocean Engineering*, 175, 1-15,
600 <https://doi.org/10.1016/j.oceaneng.2019.01.053>, 2019a.

601 Wu Z, Jiang C, Deng B, et al. Sensitivity of WRF simulated typhoon track and intensity over the South
602 China Sea to horizontal and vertical resolutions, *Acta Oceanologica Sinica*, 38(7): 74-83,
603 <https://doi.org/10.1007/s13131-019-1459-z>, 2019b.

604 Wu, Z., Jiang, C., Chen, J., Long, Y., Deng, B., and Liu, X.: Three-Dimensional Temperature Field Change
605 in the South China Sea during Typhoon Kai-Tak (1213) Based on a Fully Coupled Atmosphere–
606 Wave–Ocean Model, *Water*, 11, 140, <https://doi.org/10.3390/w11010140>, 2019c.

607 Wu, Z., Jiang, C., Conde, M., Deng, B., and Chen, J.: Hybrid improved empirical mode decomposition
608 and BP neural network model for the prediction of sea surface temperature, *Ocean Science*, 15, 349-
609 360, <https://doi.org/10.5194/os-15-349-2019>, 2019d.

610 Xiao, M., Zhang, Q., and Singh, V. P.: Influences of ENSO, NAO, IOD and PDO on seasonal precipitation
611 regimes in the Yangtze River basin, China, *International Journal of Climatology*, 35, 3556-3567,
612 <https://doi.org/10.1002/joc.4228>, 2015.

613 Xu, L., He, S., Li, F., Ma, J., and Wang, H. Numerical simulation on the southern flood and northern
614 drought in summer 2014 over Eastern China, *Theoretical and Applied Climatology*, 134, 1-13,
615 <https://doi.org/10.1007/s00704-017-2341-0>, 2018.

616 Xue, X., Chen, W., Chen, S., and Feng, J.: PDO modulation of the ENSO impact on the summer South
617 Asian high, *Climate Dynamics*, 50, 1393-1411, <https://doi.org/10.1007/s00382-017-3692-z>, 2018.

618 Yamamoto, R., Iwashima, T., and Hoshiai, M.: An analysis of climatic jump, *Journal of the Meteorological*
619 *Society of Japan. Ser. II*, 64, 273-281, https://doi.org/10.2151/jmsj1965.64.2_273, 1986.

620 Yang, L., Chen, S., Wang, C., Wang, D., and Wang, X.: Potential impact of the Pacific Decadal Oscillation
621 and sea surface temperature in the tropical Indian Ocean–Western Pacific on the variability of
622 typhoon landfall on the China coast, *Climate Dynamics*, 51, 1-11, <https://doi.org/10.1007/s00382-017-4037-7>, 2017.

623

624 Yang, J., Gong, P., Fu, R., Zhang, M., Chen, J., Liang, S., Xu, B., Shi, J., and Dickinson, R.: The role of
625 satellite remote sensing in climate change studies, *Nature climate change*, 3, 875,
626 <https://doi.org/10.1038/nclimate1908>, 2013.

627 Zhang, C., Li, H., Liu, S., Shao, L., Zhao, Z., and Liu, H.: Automatic detection of oceanic eddies in
628 reanalyzed SST images and its application in the East China Sea, *Science China Earth Sciences*, 58,
629 2249-2259, <https://doi.org/10.1007/s11430-015-5101-y>, 2015.

630 Zheng, X. T., Xie, S. P., Lv, L. H., and Zhou, Z. Q.: Intermodel uncertainty in ENSO amplitude change
631 tied to Pacific Ocean warming pattern, *Journal of Climate*, 29, 7265-7279,
632 <https://doi.org/10.1175/JCLI-D-16-0039.1>, 2016.

633 Zhou, T., Yu, R., Zhang, J., Drange, H., Cassou, C., Deser, C., Hodson, D. L. R., Sanchez-Gomez E., Li, J.,
634 Keenlyside, N., Xin, X., and Okumura, Y.: Why the western Pacific subtropical high has extended
635 westward since the late 1970s, *Journal of Climate*, 22, 2199-2215,
636 <https://doi.org/10.1175/2008JCLI2527.1>, 2009.